J|A|C|S COMMUNICATIONS

Published on Web 09/16/2009

Relating Mechanical Properties and Chemical Bonding in an Inorganic−Organic Framework Material: A Single−Crystal Nanoindentation Study

Jin Chong Tan,[†] Joshua D. Furman,[†,‡] and Anthony K. Cheetham*,[†]

Department of Materials Science and Metallurgy, University of Cambridge, Pembroke Street, Cambridge CB2 3QZ, U.K., and Materials Research Laboratory, University of California, Santa Barbara, California 93106

Received July 20, 2009; E-mail: akc30@cam.ac.uk

Crystalline framework materials that incorporate both inorganic and organic moieties are currently attracting considerable attention because their enormous chemical and structural diversity offers opportunities for creating many technologically relevant properties.[1] Much of the emphasis to date has been on nanoporous metal−organic frameworks (MOFs), which are targeted for gas separation and storage, ion exchange, catalysis, and sensing applications.[2] As has been highlighted in a recent article,[3] dense inorganic−organic hybrid frameworks have revealed a multitude of physical phenomena that are traditionally associated with purely inorganic or organic materials; these properties include photoluminescence, ferromagnetism, electronic conductivity, and nonlinear optical behavior. Notably, the dense hybrid systems often incorporate infinite inorganic connectivity, such as metal−oxygen−metal (M−O−M) arrays, that provide the topological characteristics required for certain types of physical properties.

Although a plethora of published examples of new hybrid framework materials with fascinating properties is now available, reports concerning their mechanical behavior are few. Knowledge of their ability to withstand elastic and plastic deformation is critical for applications envisaged for this new class of materials. Studies on the mechanical responses of nanoporous hybrid frameworks have started to emerge, motivated by their rapid developments toward practical applications.[4] The mechanical properties of dense hybrids, however, have remained unexplored until recently, when we published the first comprehensive study of the anisotropic mechanical properties of two copper phosphonoacetate polymorphs: $Cu_{1.5}(H_2O)(O_3PCH_2CO_2)$—the first is a three-dimensional coordination polymer and the other is a layered material with interlayer hydrogen bonding.[5] Their single crystals exhibit strikingly anisotropic mechanical responses that can be correlated to details of their crystal structures. Our findings indicate significantly higher elastic moduli along directions dominated by inorganic chains or sheets, while lower stiffnesses are prevalent along directions where the organic ligands form the primary linkages. What is not yet clear is whether it is possible to control and direct anisotropic mechanical behavior through the use of organic building blocks of varying rigidity and without affecting the M−O−M inorganic connectivity. Resolving this issue can improve our fundamental understanding of how the mechanical properties of dense inorganic−organic hybrid systems are governed by their underlying framework architectures. However, it is not possible to investigate these effects through nanoindentation of purely inorganic and organic single crystals.[6]

Here we show that the combination of organic multifunctional ligands of different rigidities can potentially be exploited to control the degree of mechanical anisotropy in a given crystallographic orientation. Our approach is to study the deformation characteristics of cerium oxalate−formate: $Ce(C_2O_4)(HCO_2)$ [**1**],[7] a lanthanide mixed-ligand hybrid which crystallizes with an orthorhombic crystal structure, as previously reported by Romero et al.[8] The three basic building blocks are the inorganic M−O−M chains and the two organic bridging ligands, namely the oxalate ($C_2O_4^{2-}$) and the formate ($HCOO^-$) ions, which are effectively oriented perpendicular to one another (Figure 1). It is also recognized that oxalate is structurally more rigid than formate.[9] This unique architecture provided us with an interesting opportunity to decouple the mechanical responses along the three primary axes by means of nanoindentation experiments and atomic force microscopy (AFM). Comparison of the elastic and plastic deformation characteristics as a function of the single-crystal orientation enables us to access the contribution associated with stiff versus compliant basic building blocks.

Compound **1** is a 3-D hybrid framework (Figure 1), and the dimensionality of its inorganic and organic connectivity are 1-D and 2-D, respectively. The 1-D inorganic chain consists of 9-coordinated cerium polyhedra that share faces to form infinite zigzag chains along the ⟨100⟩ direction. To form the 2-D organic connectivity, cerium chains are bridged by formate ligands along the ⟨010⟩ direction to form infinite 2-D layers; adjacent layers are then bridged by the oxalate ligands along the ⟨001⟩ direction to produce a 3-D framework structure.

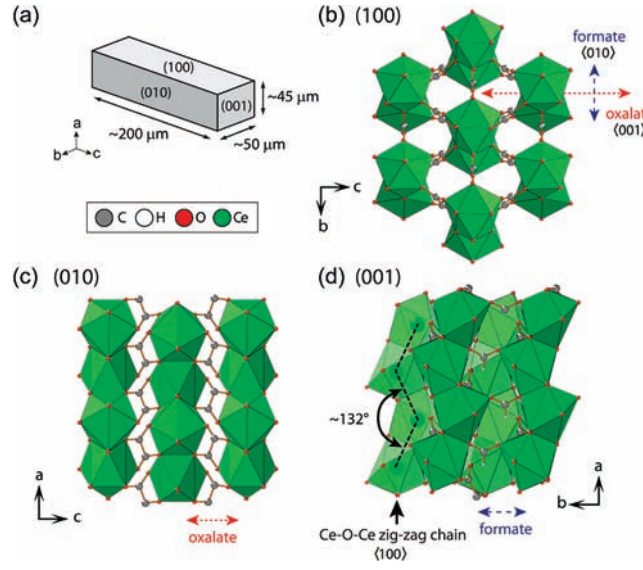

Figure 1. Crystal structure of the $Ce(C_2O_4)(HCO_2)$ hybrid framework. (a) Typical single crystal morphology (habit) and its low index faces. (b−d) Views perpendicular to the (100), (010), and (001) planes, respectively, i.e. normal to the orientation of the nanoindenter axis.

[†] University of Cambridge.
[‡] University of California.

10.1021/ja9060307 CCC: $40.75 **© 2009 American Chemical Society**

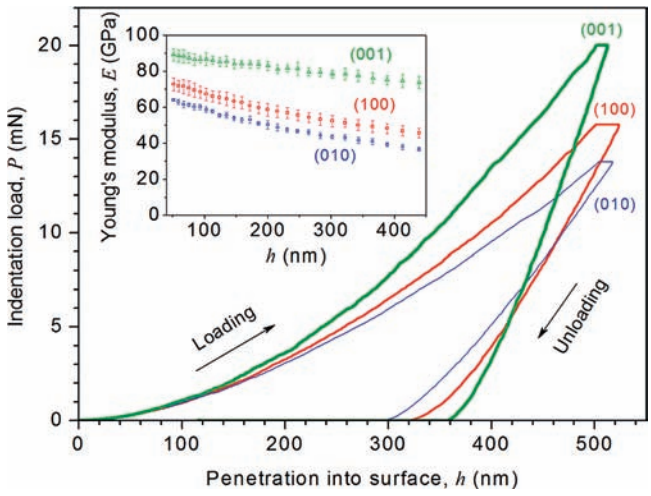

Figure 2. Results obtained from a sharp Berkovich (tetrahedral) nanoindenter showing the typical load−displacement ($P-h$) curves obtained from the three main crystallographic orientations. The inset shows the elastic (Young's) moduli data plotted as a function of surface penetration depths. The error bars correspond to standard deviations on at least 10 separate indents.

Table 1. Anisotropies of the Mechanical Properties of $Ce(C_2O_4)(HCO_2)$ from Nanoindentation Experiments Using a Berkovich Tip, As a Function of Crystallographic Orientation

	crystal facet		
mechanical properties[a]	(001)	(010)	(100)
Young's modulus, E (GPa)	78.2 ± 2.5	43.0 ± 1.4	51.8 ± 2.8
hardness, H (GPa)	4.55 ± 0.14	3.94 ± 0.06	4.11 ± 0.07

[a] All errors correspond to standard deviations on more than 10 indents.

Measurements of the directional-dependent mechanical properties of **1** were performed using a dynamic mode depth-sensing nanoindenter.[7] Tests were carried out at constant strain rate (0.05 s^{-1}) to a maximum surface penetration depth of 500 nm, with diamond indenters of two different geometries: (a) Berkovich or three-sided pyramid (tip radius ∼100 nm) and (b) a spherical tip (10 μm radius). In all cases, the indenter axes were aligned normal to the (100)-, (010)-, and (001)-oriented facets (Figure 1a), i.e. corresponding to the three primary axes of the orthorhombic unit cell.

We first consider the elastic deformation characteristics. What is immediately evident is that the load−displacement curve (Figure 2) is unique to each of the crystal facets. In particular, the maximum load sustained at full penetration depth and the degree of elastic strain recovery (at 100% unloading) are strongly dependent upon the crystallographic orientation. Such responses are direct evidence of highly anisotropic mechanical behavior. The Young's modulus (E) as a function of surface penetration depth (h), as presented in the inset of Figure 1, can be determined from the load−displacement data by applying the method of Oliver and Pharr.[10] The averaged moduli for the (001)-, (010)-, and (100)-oriented facets, measured for depths of 50 to 500 nm, are listed in Table 1. The ratio of elastic moduli for the three orthogonal orientations was found to be $E_{(001)}/E_{(010)}/E_{(100)}$= 1.82:1.00:1.20, which indicates a significant change in stiffness of greater than 80%.

We were struck by the observation that there is a straightforward correlation between the measured elastic anisotropy and the underlying chemical bonding. The (001)-oriented facet is clearly the stiffest ($E_{(001)}$ ∼78 GPa), due to the fact that rigid oxalate ligands constitute both bis-monodentate and bis-bidentate linkages that are oriented approximately parallel to the c-axis (see Figure 1c). We emphasize that this configuration coincides with the nanoindenter loading direction (i.e., down the c-axis), giving rise to a higher resistance against elastic deformation. The (010)-oriented facet, in comparison, exhibits the lowest stiffness ($E_{(010)}$ ∼43 GPa) since the bis-monodentate formate ligand, the more compliant building block within this framework, provides the primary linkages down the b-axis (see Figure 1b). These results also indicate that the oxalate ligands are clearly less effective against elastic strain when the loading axis is oriented normal to their planes. Notably, and in contrast to our recent findings,[5] the highest stiffness in **1** is not detected along the direction containing the M−O−M inorganic chains. There are two factors that may give rise to this. First, the intermediate stiffness measured on the (100)-oriented facet ($E_{(100)}$ ∼52 GPa) can partly be attributed to the Ce−O−Ce chains that zigzag down the a-axis, as defined by an angle of ∼132° between the Ce···Ce metal centers (Figure 1d). We expect that an angle approaching ∼180°, instead, would confer a higher stiffness under compression. Second, the high connectivity of the 9-coordination polyhedra is geometrically more compliant than that of the rigid 4-coordinated tetrahedra and 6-coordinated octahedra that constitute the inorganic chains in the copper phosphonoacetate hybrids studied previously.[5]

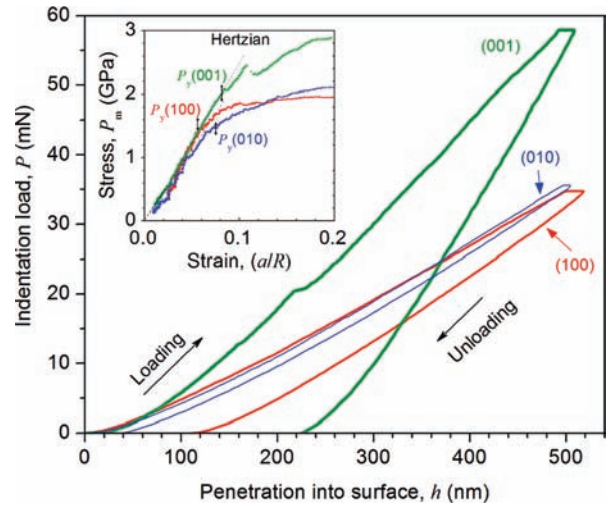

Figure 3. Typical load−displacement ($P-h$) curves obtained from spherical nanoindentation. The displacement burst or "pop-in" is generally associated with the onset of plastic deformation.[5,6d] The inset depicts the stress−strain curves derived from the $P-h$ data.[7]

We now turn to the plastic deformation characteristics. Plastic anisotropy is clearly illustrated by comparing the hardnesses (H) of the three orthogonal crystal facets (Table 1). We emphasize that the hardness of an indented crystal facet indicates its resistance against plastic flow. Specifically, it can be seen that $H_{(001)} > H_{(100)} > H_{(010)}$, in which the (001)-oriented facet appears to be the hardest and the maximum change in hardness is ∼15%.

To elucidate the underlying plastic mechanisms, we now consider the spherical-tipped nanoindentation data (Figure 3). The strain field induced by a large curvature is less localized, and this delays the onset of plasticity allowing the elastic−plastic transition to be captured.[11] Consequently, maximum loads of greater than a factor of 2 may develop during loading, although this is accompanied by substantial elastic recovery upon unloading. To illustrate this further, Figure 4 presents the AFM height topology of residual indents made on the (001) facets, using the two different nanoindenter tip geometries. The extent of elastic recovery experienced by the (010)-oriented plane was found to be unusually high, in which the elastic portion of the indentation work (W_{el}) can easily surpass 90% (see

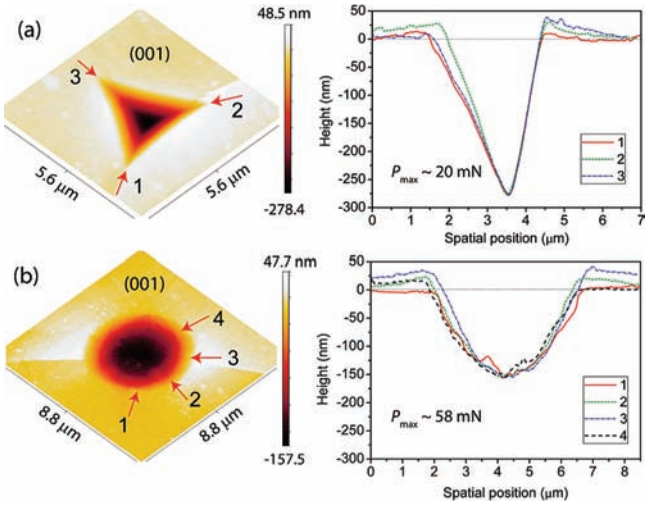

Figure 4. AFM height topology of the residual indents to a maximum depth of 500 nm on the (001)-oriented facet, under a (a) Berkovich and (b) spherical indenter. Their corresponding cross-sectional profiles along the designated paths are plotted on the right.

Table S2 for full data[7]). Since the geometry of a spherical tip is not self-similar, the contact strain generated is constantly changing as a function of penetration depth. Such load−displacement data can be clearly represented as an indentation stress−strain curve,[7] as shown in the inset of Figure 3. The yield pressure (P_y) denotes the critical stress that corresponds to the onset of plastic deformation (i.e., point of deviation from Hookean linearity). We note that the (001)-oriented facet exhibits the highest yield pressure (~2 GPa), while those corresponding to the (100)- and (010)-oriented planes are relatively lower at ~1.4 and ~1.2 GPa, respectively. In terms of the yielding response, we obtained $P_{y\ (001)} > P_{y\ (100)} > P_{y\ (010)}$, consistent with Tabor's relation $H = C \cdot P_y$,[12] whereby the hardness scales with the yield pressure (the proportionality constant C varies with the crystal facets due to single crystal anisotropy).

It is certainly worth noting that the shape of the stress−strain (P_m vs a/R) curves (Figure 3 inset) indicates the type of strain-hardening response that dominates in each crystallographic orientation. The (001) plane exhibits a power-law hardening behavior (i.e., of the form $P_m \propto (a/R)^n$, where n is the strain exponent) that is commonly associated with dislocation entanglement. In contrast, the (100)- and (010)-oriented planes both show a perfectly plastic response, with a plateau at ~2 GPa. Here, the absence of strain hardening response highlights the lack of dislocation interactions. The different strain hardening behavior can also be correlated to the extent of pile-up developed around the indents (see Figure S4[7]). Beyond the elastic limit, it is always challenging to make any direct correlations between the crystal structure and the observed plastic behavior.[6a,13] At this stage, we reason that the rigid oxalate ligands down the c-axis are also contributing toward the greater hardness, yield pressure, and strain-hardening response detected in the (001)-oriented face. This may partly be attributed to the fact that the two slip systems present in an orthorhombic crystal system, viz. {010} ⟨100⟩ and {010} ⟨001⟩,[14] are both orthogonal to the indented (001) plane. It is now part of our future plans to understand the detailed plastic deformation mechanisms of crystalline hybrid systems by studying the dislocation activities in the plastic zone using transmission electron microscopy (TEM).

In conclusion, this study has brought us one step closer toward understanding the complex structure−mechanical property relationships in crystalline hybrid framework materials. We have demonstrated that the directional compressive strain generated by the diamond indenter tip offers a unique means to establish the anisotropic deformation characteristics in the elastic and plastic domains. This study presents the first conclusive evidence that the crystal orientation dominated by inorganic chains is not necessarily more robust from the mechanical properties standpoint. Evidently, rigid organic bridging ligands (e.g., oxalate), when strategically oriented, can give rise to greater stiffness and hardness properties and hence influence the degree of mechanical anisotropy. On this basis, and in view of the diverse structural and chemical variability of hybrids, we anticipate that there exists a vast opportunity to "design" mechanical properties, potentially via a crystal engineering approach.[15] Our results clearly reveal the fundamental relationships between the nature of chemical bonding and the anisotropic mechanical responses of dense hybrid frameworks.

Acknowledgment. We thank the Cambridge Newton Trust (J.C.T.), Mitsubitshi Chemicals Corporation (J.D.F.), and the European Research Council for providing financial support. The authors are grateful to Dr. J. B. Orton and the EPSRC UK National Crystallography Service for single-crystal X-ray diffraction experiments. J.C.T. would also like to thank Dr. A. Thirumurugan for a number of productive scientific discussions.

Supporting Information Available: Synthetic methods, crystallographic information file (CIF), nanoindentation and AFM experimental procedures, and nanoindentation data analyses. This material is available free of charge via the Internet at http://pubs.acs.org.

References

(1) (a) Cheetham, A. K.; Rao, C. N. R.; Feller, R. K. *Chem. Commun.* **2006**, 4780–4795. (b) Rao, C. N. R.; Cheetham, A. K.; Thirumurugan, A. *J. Phys. Condens. Matter.* **2008**, *20*, 083202. (c) Kurmoo, M. *Chem. Soc. Rev.* **2009**, *38*, 1353–1379. (d) Allendorf, M. D.; Bauer, C. A.; Bhakta, R. K.; Houk, R. J. T. *Chem. Soc. Rev.* **2009**, *38*, 1330–1352. (e) Jain, P.; Dalal, N. S.; Toby, B. H.; Kroto, H. W.; Cheetham, A. K. *J. Am. Chem. Soc.* **2008**, *130*, 10450–10451.
(2) (a) Férey, G. *Chem. Soc. Rev.* **2008**, *37*, 191–214. (b) Kitagawa, S.; Kitaura, R.; Noro, S. *Angew. Chem., Int. Ed.* **2004**, *43*, 2334–2375. (c) Czaja, A. U.; Trukhan, N.; Muller, U. *Chem. Soc. Rev.* **2009**, *38*, 1284–1293. (d) Banerjee, R.; Phan, A.; Wang, B.; Knobler, C.; Furukawa, H.; O'Keeffe, M.; Yaghi, O. M. *Science* **2008**, *319*, 939–943. (e) Rosseinsky, M. J. *Microporous Mesoporous Mater.* **2004**, *73*, 15–30. (f) Murray, L. J.; Dinca, M.; Long, J. R. *Chem. Soc. Rev.* **2009**, *38*, 1294–1314.
(3) Cheetham, A. K.; Rao, C. N. R. *Science* **2007**, *318*, 58–59.
(4) (a) Spencer, E. C.; Angel, R. J.; Ross, N. L.; Hanson, B. E.; Howard, J. A. K. *J. Am. Chem. Soc.* **2009**, *131*, 4022–4026. (b) Chapman, K. W.; Halder, G. J.; Chupas, P. J. *J. Am. Chem. Soc.* **2008**, *130*, 10524–10526. (c) Allendorf, M. D.; Houk, R. J. T.; Andruszkiewicz, L.; Talin, A. A.; Pikarsky, J.; Choudhury, A.; Gall, K. A.; Hesketh, P. J. *J. Am. Chem. Soc.* **2008**, *130*, 14404–14405. (d) Bahr, D. F.; Reid, J. A.; Mook, W. M.; Bauer, C. A.; Stumpf, R.; Skulan, A. J.; Moody, N. R.; Simmons, B. A.; Shindel, M. M.; Allendorf, M. D. *Phys. Rev. B* **2007**, *76*, 184106.
(5) Tan, J. C.; Orton, J. B.; Merrill, C. A.; Cheetham, A. K. *Acta Mater.* **2009**, *57*, 3481–3496.
(6) (a) Kearney, C.; Zhao, Z.; Bruet, B. J. F.; Radovitzky, R.; Boyce, M. C.; Ortiz, C. *Phys. Rev. Lett.* **2006**, *96*, 255505. (b) Lethbridge, Z. A. D.; Williams, J. J.; Walton, R. I.; Smith, C. W.; Hooper, R. M.; Evans, K. E. *Acta Mater.* **2006**, *54*, 2533–2545. (c) Reddy, C. M.; Gundakaram, R. C.; Basavoju, S.; Kirchner, M. T.; Padmanabhan, K. A.; Desiraju, G. R. *Chem. Commun.* **2005**, 3945–3947. (d) Viswanath, B.; Raghavan, R.; Ramamurty, U.; Ravishankar, N. *Scripta Mater.* **2007**, *57*, 361–364.
(7) Full details can be found in the Supporting Information.
(8) Romero, S.; Mosset, A.; Trombe, J. C. *J. Solid State Chem.* **1996**, *127*, 256–266.
(9) Rao, C. N. R.; Natarajan, S.; Vaidhyanathan, R. *Angew. Chem., Int. Ed.* **2004**, *43*, 1466–1496.
(10) (a) Oliver, W. C.; Pharr, G. M. *J. Mater. Res.* **2004**, *19*, 3–20. (b) Oliver, W. C.; Pharr, G. M. *J. Mater. Res.* **1992**, *7*, 1564–1583.
(11) Swain, M. V. *Mater. Sci. Eng., A* **1998**, *253*, 160–166.
(12) Tabor, D. *Philos. Mag. A* **1996**, *74*, 1207–1212.
(13) Lloyd, S. J.; Castellero, A.; Giuliani, F.; Long, Y.; McLaughlin, K. K.; Molina-Aldareguia, J. M.; Stelmashenko, N. A.; Vandeperre, L. J.; Clegg, W. J. *Proc. R. Soc. Edinburgh, Sect. A: Math.* **2005**, *461*, 2521–2543.
(14) Hebbache, M. *Solid State Commun.* **2000**, *113*, 427–432.
(15) (a) Robson, R. *J. Chem. Soc., Dalton Trans.* **2000**, 3735–3744. (b) Robson, R. *Dalton Trans.* **2008**, 5113–5131. (c) Yaghi, O. M.; O'Keeffe, M.; Ockwig, N. W.; Chae, H. K.; Eddaoudi, M.; Kim, J. *Nature* **2003**, *423*, 705–714.

JA9060307